Evolution of disorder in magnetic stripe domains. II. Hairpins and labyrinth patterns versus branches and comb patterns formed by growing minority component

M. Seul and R. Wolfe
AT&T Bell Laboratories, Murray Hill, New Jersey 07974
(Received 13 May 1992)

An analysis is presented of the role of topological defects in the evolution of disordered stripe-domain phases of ferrimagnetic garnet films. Proliferation by continued nucleation and topologically constrained unbinding of disclination dipoles are identified as the essential mechanisms mediating the strain-induced disordering process. Two distinct classes of metastable, disordered states are distinguished on the basis of the relative predominance of defect-pair proliferation and unbinding, and the fundamentally different corresponding pattern morphologies which accommodate the emerging disclination network. Striking patterns containing linear chains of interdigitated disclination dipoles are representative of the first class, while labyrinthine patterns, exhibiting a robust and well-defined local structure in the form of "cybotactic" clusters, are typical of the second class. Results are discussed with reference to defect-mediated melting and the structure of glasses. Comparison is also made with pertinent phenomena in related systems such as ferrofluids and amphiphilic films.

PACS number(s): 64.60.−i, 05.70.Fh, 64.70.−p, 75.70.Kw

I. INTRODUCTION

A. Disordering of modulated phases

Domain formation in a wide variety of condensed-matter systems has been accounted for by invoking the concept of competing interactions. Specifically, in thin films of such materials as ferroelectrics [1], type-I superconductors [2], ferrofluids [3] and ferrimagnetic garnets [4, 5], as well as more recently in Langmuir films—that is, monomolecular amphiphilic layers adsorbed at an air-water interface [6]—formation, shapes, and stability of domains have been attributed to the competition based on an attractive interaction of short range, i.e., a domain-wall energy, and a repulsive interaction of electrostatic or magnetostatic origin and hence of long range. That is, domain formation has been interpreted as an indication of the condensation of the system in a modulated phase, the simplest realizations of which are unidirectionally modulated "stripe" and trigonally modulated "bubble" phases explicitly incorporated in mean-field theories of Langmuir monolayers [7] and magnetic garnets [8]. The modulation period of the pertinent order-parameter field is set by the balance of the competing interactions and generally depends on temperature and externally applied field(s), as discussed in the preceding article, referred to as I in what follows, which also contains the generic mean-field diagram constructed on the basis of the concept just introduced, as well as actual examples of the realization of these ordered ground states.

In contrast to what is assumed in the simplest mean-field-theory solutions, the patterns most frequently encountered in experiments are disordered. This is particularly so in the case of stripe patterns for which "labyrinthine" morphologies have been reported in most of the systems enumerated above [1–3,5,9–11]. Comparatively little effort has been directed at the elucidation of the mechanisms governing the evolution of disorder in spite of the expectation that, given the common basis of theoretical description for a wide range of realizations of modulated phases, such mechanisms would likely be of quite general relevance. In the context of thin ferrofluid films, a variety of studies were undertaken by Tsebers and Maiorov [11], as well as Rosensweig, Zahn, and Shumovich [12], and the problem is now receiving increased experimental and theoretical attention motivated by the desire to understand the evolution of complex labyrinthine shapes within a generally valid mathematical framework [13]. In the context of magnetic garnet films, Molho and collaborators initiated a systematic study of the role of topological characteristics of stripe patterns. Thus, they investigated pattern evolution under magnetic-field and temperature cycling [14], and explored the effects of introducing perturbations of the optimal modulation period of the pattern [15]. More recently, the defect-mediated melting of an ordered magnetic bubble array has been investigated in quantitative detail [16]. The problem of stripe-phase melting in these effectively two-dimensional systems is of related interest, particularly in view of observations of a "stripe liquid" in Langmuir monolayers [17]; recent experiments directly addressing this issue [18] have in fact located a transition to an ordered state closely resembling the two-dimensional nematic phase, predicted by defect-mediated melting theory [19,20] to emerge as a highly defected smectic phase [21], as discussed in the preceding article I.

The evolution of labyrinthine patterns from two well-defined initial states constitutes the topic which we will discuss in detail in the present article, with particular focus on the role of topological defects in the disordering process. In I we describe the evolution of a lamellar pattern under temperature-induced strain along the symmetry axis ($H=0$) of the phase diagram. Here we investigate the mechanisms by which globally disordered

stripe-domain states in ferrimagnetic garnet films evolve in response to magnetic-field-induced strain. Primary attention is thus given to the evolution along an experimental trajectory originating in a uniformly magnetized initial state from which individual "meandering" stripes nucleate and proceed, under demagnetization at constant temperature, to fill the available sample area. We rely on the extensive application of algorithms for line-pattern analysis to elucidate the essential role played by "nucleation" and "unbinding" of defect pairs in this process. The evolution of disorder is driven by strain, imposed on a given pattern by means of tuning the characteristic modulation wave vector via its magnetic-field and temperature dependence. Strain is the relevant experimental variable and, as we will discuss, the mechanism of disclination unbinding displays identical characteristics irrespective of whether patterns evolve in response to field-induced strain, as in the experiments discussed here, or in response to temperature-induced strain, the situation realized in the experiments reported in I. A portion of our results has been previously reported in abbreviated form [22,23].

B. Summary and outline

In article I, particular attention was given to the problem of period adjustment in a lamellar state and to the transverse pattern instabilities which mediate the lamellar state's response when subjected to temperature-induced dilative strain; this arises from the constraint that the number of lamellae present in the system cannot be increased as required to accommodate, within the lamellar configuration, the period reduction implied by increasing temperature. The appearance of undulation and chevron patterns is broadly consistent with a local elastic response of the magnetic stripe pattern, as proposed in a recent theory [24] and establishes a direct analogy between the magnetic lamellae, an effectively two-dimensional system, and smectic liquid crystals [25,26]. The accumulation of strain eventually destabilizes the emerging chevron pattern by a process of defect-pair nucleation. The subsequent unbinding of these defects will be given more explicit attention here.

Our principal observations may be summarized as follows. Disordered stripe patterns contain topological defects which are introduced in the evolving pattern in the form of disclination dipoles and are indicative of stripe or line branching. Under conditions of slowly increasing strain, existing disclination dipoles undergo a continuous "unbinding" transition. This entails the motion of disclinations of opposite charge, initially paired into a dipole, to uncorrelated positions. This motion follows a trajectory marked in the pattern by a curvilinear connecting contour, or "tether" [22]. The fact that line rupture ("pinchoff") and intersection are forbidden for the range of experimental parameters relevant here, and in contrast to the fluctuation-dominated behavior of certain Langmuir monolayers [17,18], constitutes a strong topological constraint on the evolving pattern in the form of its global connectivity. Consequently, disordered stripe patterns generally represent the realization of a constrained minimization of the pertinent free energy and are in this sense metastable. The disclination-pair unbinding contemplated here is thus distinct from the defect-pair unbinding considered by Kosterlitz and Thouless [27] and analyzed in the context of defect-mediated melting [19,20,28,29]. It may be more appropriately regarded as a fundamental process mediating the evolution of amorphous structure in stripe phases. Disclination-dipole unbinding leads to the appearance of a globally disordered "labyrinthine" state with a well-defined local structure, based on a prominent motif in the form of oblong polygonal clusters of ordered stripe segments, and characterized by a density n_D of disclinations defining an "intermediate" length scale, $\xi \sim n_D^{-1/2}$, related to the characteristic size of segment clusters [23]. As shown in a related article [30], extensive statistical analysis of numerous structural attributes of such segment clusters reveals these to be remarkably robust and independent of the choice of trajectory in the magnetic-field–temperature phase diagram.

Demagnetization at a fixed temperature from a state of saturated magnetization leads to a labyrinthine pattern via the elongation of a single (or a small number of) "meandering" stripe(s) of the invading ("minority") component. These stripes elongate without rupturing or branching, thereby confining disclination dipoles completely to the "majority" component. Hairpin turns figure prominently in the self-avoiding configurations of the evolving stripe(s). The resulting disordered state appears to represent a deep local minimum in the free energy of the stripe pattern which is reached under "adiabatic" conditions of increasing strain whenever topological constraints prevent access to the lamellar pattern representing the state of globally minimal free energy [23,30].

In contrast, the proliferation of defects by continued nucleation predominates in response to rapidly increasing, magnetic-field-induced strain, favoring the formation of highly branched, metastable stripe configurations. Striking patterns, composed of ordered arrays of alternating disclination dipoles, are observed in this situation. The competition between nucleation and unbinding of disclination pairs is shown to be biased by the rate of external "forcing," that is, in the present context, the rate of change of magnetic-field-induced strain, relative to the rate at which local strain is accommodated via transverse motion of domain walls as the stripe period evolves. These findings suggest the existence of distinct classes of metastable, amorphous structures, distinguished by the relative preponderance of branching over defect-dipole-unbinding events in the course of disordering. We argue that the morphology reflects the local strain distribution during the evolution of disorder.

The remainder of this article is organized as follows. In Sec. II we provide a description of experimental apparatus and procedures; a detailed discussion of the methods of digital image and pattern analysis employed here is given elsewhere [30]. Section III contains the bulk of our results pertaining to the evolution of disordered patterns from well-defined initial states. In particular, we examine the case of magnetic-field-induced strain. The

discussion of these findings in Sec. IV is guided by reference to concepts from the theory of defect-mediated melting as well as to the description of amorphous structure. Comparison is also made with pertinent phenomena in related systems—notably ferrofluidic and amphiphilic films.

II. MATERIALS AND EXPERIMENTAL PROCEDURES

A. Garnet films

Experiments were performed on thin, transparent films of magnetic garnet, grown by liquid-phase epitaxy on single-crystal substrates of gadolinium gallium garnet (GGG) of (111) orientation. Garnet crystals have cubic symmetry, with 160 atoms per unit cell arranged in a complex structure. These crystals were prepared without dislocations in the form of 2-in. diameter wafers. The epitaxial films were sufficiently thin to eliminate closure domains of magnetization near the surface [4,31]; in the present case, a thickness of about 13 μm was chosen. Their composition, $(YGdTm)_3(FeGa)_6O_{12}$, was confirmed by means of x-ray fluorescence analysis.

These magnetic garnet materials, originally produced to study their potential application in a variety of devices such as computer "bubble" memories, are ferrimagnetic and contain two opposing iron sublattices. The large amount of gallium on the majority iron site reduces the magnetic moment to a low value ($4\pi M_s \sim 70$ G at room temperature), resulting in relatively large domains for enhanced visibility. The substitution of rare-earth ions on the yttrium sites gives rise to a large, growth-induced uniaxial anisotropy with the easy axis of magnetization perpendicular to the plane of the film. The field required to saturate the films parallel to the surface is a factor of about 30 larger than the perpendicular saturation field. The films therefore exhibit the behavior of an Ising ferromagnet over a wide temperature range, with alternating domains of "up" and "down" magnetization in the characteristic "stripe" and "bubble" configurations. In spite of their intricate atomic structure, (111) films with uniaxial magnetic anisotropy are isotropic in the plane, i.e., there is no preferred orientation of domain walls. Extremely low coercivities were achieved, ensuring low friction and smooth domain-wall motion, particularly at elevated temperatures.

B. Experimental arrangement and procedures

Samples approximately 10 mm$\times$10 mm in size were cut from the original wafers and placed into a small, ceramic (Al_2O_3) furnace of cylindrical shape, heated via a 10-Ω bifilar winding (Minco Products, Minneapolis, MN) and equipped on top and bottom with double-paned windows (Meadowlark Optics, Longmont, CO), also employed in a commercial microscope hot stage (Instec, Boulder, CO). Temperature control (DRC 91C, Lake Shore Cryotronics, Westerville, OH) relied on a 100-Ω Pt resistance temperature device (RTD) (Omega Engineering, Stamford, CT) cemented to an interior wall of the furnace; the actual temperature was monitored in close proximity to the garnet film by reading a 10-$k\Omega$ thermistor (YSI, Yellow Springs, OH) into a high-resolution digital voltmeter (HP 3456A, Hewlett Packard, Palo Alto, CA). The furnace was designed to fit into the 1-$\frac{1}{2}$-in.-diam bore of an air-cooled solenoid of 2-$\frac{1}{2}$ in. length, capable of generating an axial magnetic field of up to approximately 500 Oe. Fields were calibrated using a solid-state Hall sensor (SS94A1, MicroSwitch, Freeport, IL) in place of the sample; the pertinent resolution, achieved via an analog controllable power supply (HP6269B, Hewlett Packard, Palo Alto, CA) was approximately 1 Oe.

The entire assembly, sketched in Fig. 1, was placed on a stage to fit a standard Zeiss Universal microscope, equipped for polarization microscopy, and aligned for Koehler illumination [32]. The observation of domains of magnetization relies on the Faraday effect, that is, the rotation of the plane of polarization of light transmitted through the film in a direction parallel or antiparallel to that of the magnetization. A charge-coupled device (CCD) video camera with external control of gain and black level (CCD 72, Dage MTI, Michigan City, IN) permitted us to take advantage of well-known contrast and resolution enhancement [33]. In addition, time-resolved video microscopy was aided by employing an optical memory disk recorder (TQ-2028F, Panasonic, Secaucus, NJ) facilitating frame-by-frame analysis of rapidly evolving patterns [34].

The source of illumination was usually a standard 100-W Hg lamp, in combination with a flat-field corrected condenser of numerical aperture (NA) 0.32 (Zeiss, Thornwood, NY), matched to the NA of the normally employed flat-field corrected objectives of NA 0.1 (4$\times$) to NA 0.3 (10$\times$) (Wild-Leitz, Rockleigh, NJ). Diffraction spectra were recorded by imaging the depolarized component of the input illumination, in this case provided by

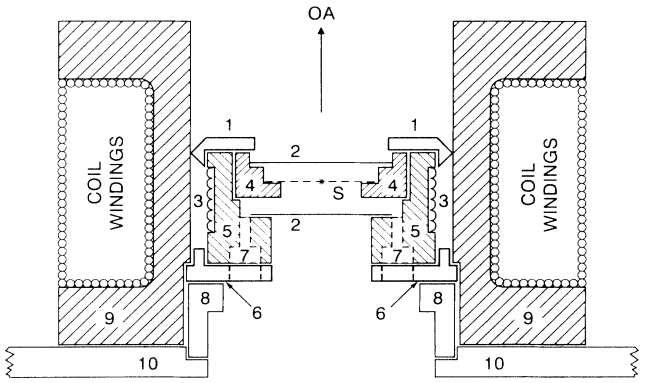

FIG. 1. Experimental assembly, shown in side view, containing the ceramic furnace, surrounded by a solenoid, as described in Sec. II B of the text. OA, optic axis; S, sample; 1 and 6, thermally insulating end caps, also serving as locating devices, machined from Vespel (DuPont, Wilmington, DE); 2, double-paned windows (see Sec. II B); 3, bifilar winding; 4, removable top piece of ceramic furnace; 5, body of ceramic furnace, machined from alumina ceramic (Cotronics, Brooklyn, NY); 7, feedthroughs; 8, aluminum spacer; 9, solenoid, of 4-in. diameter, machined from Macor (Corning, Corning, NY); 10, aluminum baseplate.

the 514-nm line of an argon-ion laser (Innova 90-5, Coherent, Palo Alto, CA), in the back focal plane of a 10×, NA 0.3 objective. This is accomplished by means of a Bertrand lens inserted in the optical train of the microscope.

Computer control of all measurement and video recording functions allowed for convenient and reproducible ramping of temperatures and magnetic fields and the capture of images as well as experimental parameters on videotape for subsequent analysis. A detailed exposition of the methods of digital pattern analysis is given elsewhere [30].

III. EVOLUTION OF LABYRINTHINE STRIPE-DOMAIN PATTERNS IN RESPONSE TO MAGNETIC-FIELD-INDUCED STRAIN

In this section we elaborate on the findings briefly summarized in Sec. I. Invoking extensive digital line-pattern analysis, we examine in detail the mechanisms mediating the evolution of disorder in stripe-domain states and the formation of several types of labyrinthine patterns.

In all experiments analyzed here, disordering is driven by externally imposed strain, controlled via the magnetic-field [5] dependence of the characteristic modulation wavevector, $q=q(H,T)$, described in Sec. III A of I. In particular, we note that, over the range of parameters relevant to the present report, temperature is not a relevant variable: No fluctuation effects are in evidence, in contrast to what is observed in the "critical" region [35].

A. Disclination unbinding in response to field-induced strain

According to the temperature dependence of the stripe period, d, discussed in Sec. III A of I and sketched there in Fig. 1, the largest variation in temperature-induced strain is achieved near the mean-field critical temperature. However, image contrast is due to the Faraday effect and vanishes with decreasing magnetization amplitude, rendering difficult the recording of patterns with high contrast in the critical region. Conversely, the stripe period may be varied over a large range, i.e., by a factor of 2 to 3, via its dependence on magnetic field, also sketched in Fig. 1 of I. To record data for a detailed analysis of the unbinding process as well as for the study of kinetic effects on defect proliferation, to be described in Sec. III B, it proved to be advantageous to rely on magnetic-field-induced strain, as discussed in what follows.

Figure 2 contains a sequence of stripe configurations representing intermediates in the transformation of a labyrinthine into a lamellar stripe pattern. That is, the sequence was actually recorded in reverse order from that displayed: Starting with the labyrinthine pattern in Fig. 2(d), generated from an initial lamellar state via *temperature*-induced strain accumulation as discussed in I, the return of the pattern to the ordered lamellar state was accomplished by relieving the stored strain via the magnetic-field dependence of the stripe period. In this sense, temperature and external magnetic field are completely equivalent within the respective ranges pertinent to the present experiments: Both serve as a means to vary the stripe period d.

It should be noted that the sequence of transformations depicted in Fig. 2 is completely reversible, provided that disclination dipoles are not actually annihilated. That is, if the field is raised to sufficiently high values to decrease stored strain below the yield threshold, disclination pairs vanish and a lamellar state eventually appears, here at $H\simeq 0.95H_{\rm sat}$ with $H_{\rm sat}(T=150\,^{\circ}\mathrm{C})\simeq 65$ Oe. A return to the branched labyrinth, otherwise accomplished by lowering the field back to $H=0$, then becomes impossible: Instead, a banded labyrinth is formed, exhibiting a completely asymmetric distribution of disclinations between its two components [22,23,30].

The left-hand column of Fig. 2, containing panels (a)–(d), has been previously presented [22]. It is the configuration of the "tethers" joining oppositely charged disclinations as shown in the figure's right-hand column which permits the identification of global descriptors capturing the essence of the disclination-pair unbinding transition. Thus, it is apparent that in the course of the evolution of disorder, the tether contour is greatly elongated, while, concomitantly, its shape becomes increasingly irregular. That is, the trajectory of the path between joined countercharges is transformed from a straight line characterizing disclination dipoles into a meandering contour.

A detailed shape analysis of the tether trajectory is possible on the basis of a variety of measures employed in the theory of random flights [36], also briefly alluded to elsewhere [30]. Here, we have relied on a quantitative description of the dipole unbinding process in terms of two simple global descriptors of the tether contour, namely, the contour length l and the ratio $d_{\rm ee}/l$ of end-to-end distance and contour length. These two quantities capture essential features of the unbinding process as identified above: contour elongation and "randomization" of orientation. Given a sample of sufficient size, comparison of the behavior of the ratio $d_{\rm ee}/l$ with pertinent results from the study of polymer chain statistics [37] and nonintersecting space filling walks [38] may be of interest. Results obtained by analyzing the data set from which the configurations in Fig. 2 were drawn have been presented elsewhere [22]. In Fig. 3 we summarize the analysis of a second data set, recorded under similar experimental conditions. Comparison with the earlier analysis is gratifying, because it reveals that the description chosen here is quite robust, yielding virtually identical behavior for the evolution of both $\langle l\rangle$ and $\langle d_{\rm ee}/l\rangle$ as a function of dilative strain $\epsilon\equiv(d_0-d)/d_0$.

The behavior of $\langle l\rangle$ may be understood from the following argument, based on the assumption of stripe elongation. Consider an Archimedean spiral (of constant curvature) in a circular area of radius $R_0\simeq Nd$; if $r(\phi)=(d/2\pi)\phi$, the spiral will complete N revolutions as its radius increases to R_0. The contour length l may be estimated in the form

$$l=\sum_{n=0}^{N-1}L_n,\quad L_n=\int_{n2\pi}^{(n+1)2\pi}r(\phi)d\phi\ .$$

With $r=r(\phi)$ from above, one has $l_n=\pi d(2n+1)$ and

$l \sim \pi d N^2$; given $N = R_0/d$, this implies $l \sim 1/d$. That is, we expect the total contour length to increase linearly as the period d decreases. Application of this argument to the elongation of tether contours joining oppositely charged disclinations suggests a linear functional form: $l = ad^{-1} + b$. In general, $b \neq 0$, reflecting the experimental observation that l, the tether contour length, vanishes at some finite value d^* of the period. For $l = 0$, $b = -a/d^*$; hence, $l = a(1/d - 1/d^*)$ and $ld \sim (d^* - d)/d^*$. That is, the product ld is expected to

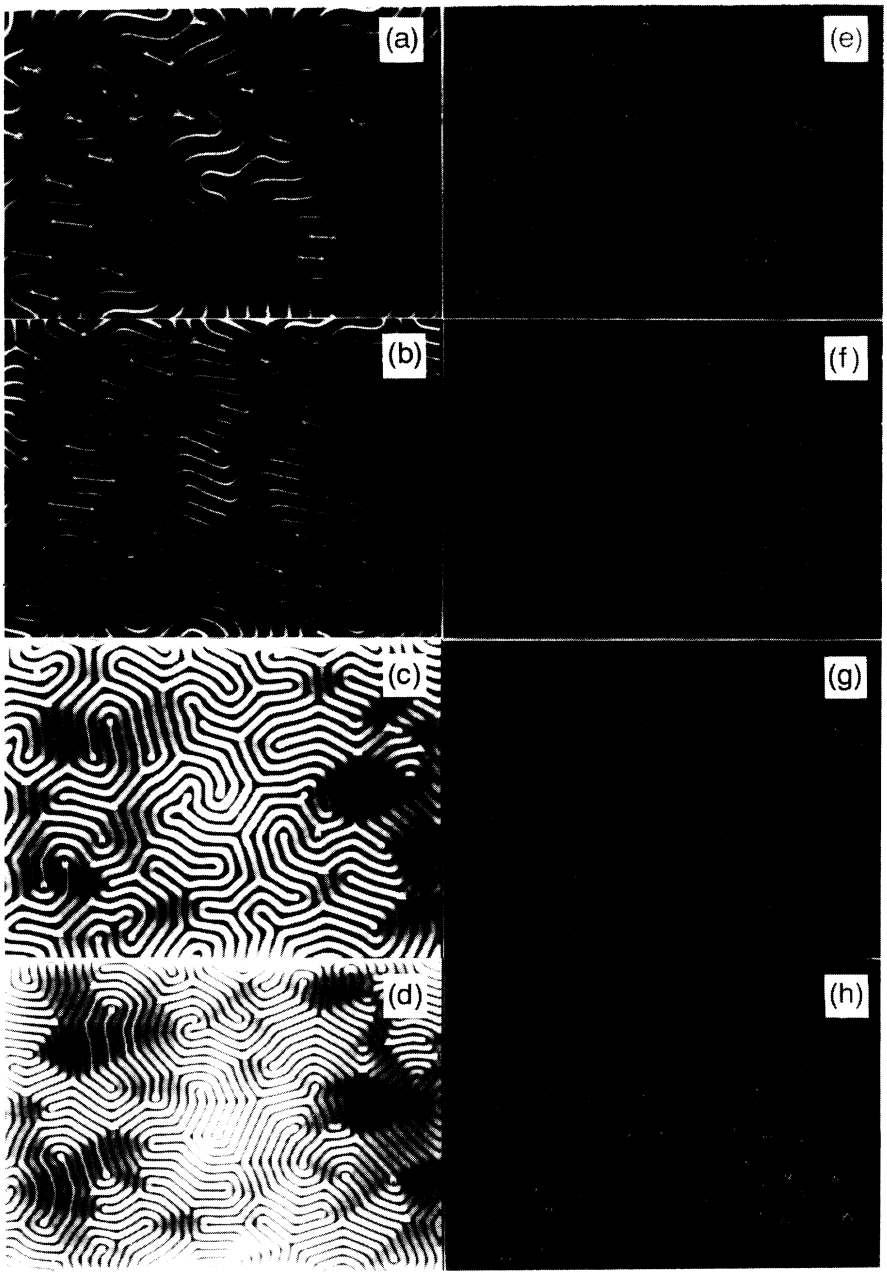

FIG. 2. Intermediate states in the course of disclination-dipole unbinding, formed in response to magnetic-field-induced dilative strain; $T = 160\,^{\circ}\mathrm{C}$ ($\simeq 0.8 T_c$). The bottom row depicts a branched labyrinth pattern at $H = 0$ Oe. Preceding the pattern in the top row is a lamellar pattern, not shown here. The right-hand column contains $-\frac{1}{2}$ ("Δ") and $+\frac{1}{2}$ ("○") disclinations as well as the connecting tether, identified in the corresponding stripe pattern by a set of algorithms for line-pattern analysis [30]. In the left-hand column, disclination charges ("Δ," "○") and the connecting tethers are superimposed on the original stripe pattern [22]. The stripe patterns displayed in the two lower panels on the left were treated by application of low-pass and dilation filters. The shading so generated makes it readily apparent that disclinations are located along the boundaries of "segment" clusters, i.e., order regions composed of parallel stripe segments [23,30]. An analysis of this data set has been previously presented [22]. The horizontal dimension of each field of view is 570 μm.

scale linearly with dilative strain ϵ, evaluated with respect to the reference state with $d=d^*$.

In constructing the linear fit to the data in Fig. 3, we have simply equated d^* with d_0. This is justified if one considers the value of d obtained by extrapolating the linear portion of the plot to $l=0$. As may be judged from the figure, the linear fit captures the essence of the operative disordering mechanism. In this context, it is important to note a crucial assumption on which the validity of the linear scaling of $ld \sim \epsilon$ is based: The nucleation of additional disclination dipoles in the course of the unbinding process is neglected. The contribution from such a mechanism to strain relief would result in a sublinear dependence of l on $1/d$. A dramatic realization of this expectation will be discussed in Sec. III B in connection with the highly branched, interdigitated "comb" patterns of Figs. 4 and 5. For the cases analyzed here, we conclude that the evolution of disorder is mediated primarily by disclination-dipole unbinding, that is, by elongation of tether contours.

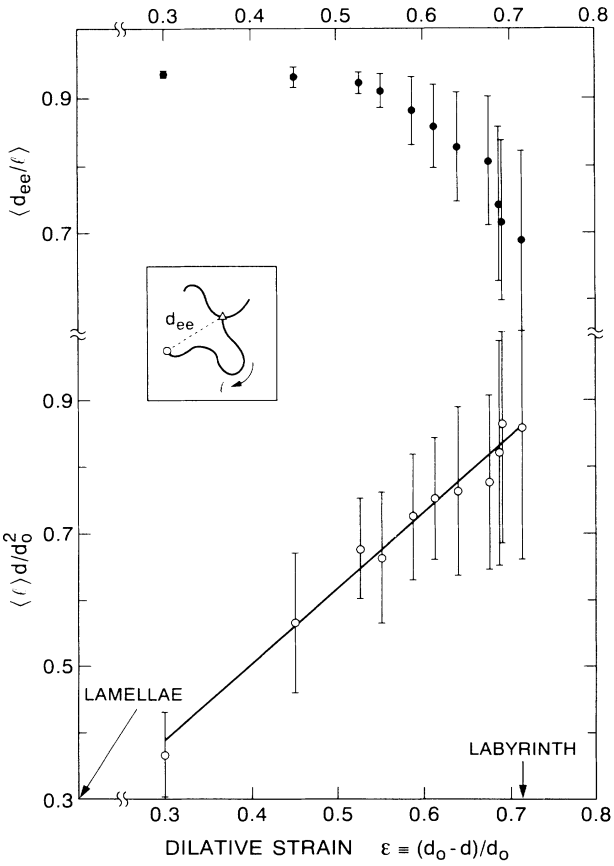

FIG. 3. Analysis of magnetic-field-induced disclination unbinding at $T=160\,^{\circ}\mathrm{C}$ ($\simeq 0.8T_c$), in terms of two global descriptors of the curvilinear contour ("tether") joining $-\frac{1}{2}$ and $+\frac{1}{2}$ disclination charges, namely, the tether contour length $\langle l \rangle$ and the ratio $\langle d_{ee}/l \rangle$ of end-to-end distance d_{ee} to contour length. Displayed is the dependence of both quantities on dilative strain, $\epsilon \equiv (d_0-d)/d_0$; here, d_0 denotes the stripe period of the lamellar stripe pattern realized at high magnetic field, as discussed in the text. The solid line in the lower plot results from a linear fit, suggested by a scaling argument discussed in Sec. III A of the text. Vertical bars indicate $\pm\frac{1}{2}\sigma$, σ denoting the standard deviation; $\langle\ \rangle$ implies an average over a field of view (see, e.g., Fig. 2).

Importantly, elongation is accompanied by a continuously advancing "randomization" of the tether contour orientation: Straight connecting tethers evolve into meandering, self-avoiding curves. This is the content of the plot displaying the dependence of $\langle d_{ee}/l \rangle$ on dilative strain. The randomization constitutes an essential element in the disordering, because it leads to the complete loss of globally preferred directions of the pattern, with corresponding Fourier spectra ultimately exhibiting complete global averaging, as discussed in related articles [23,30]. No theoretical understanding of this process currently exists. Similarly, the continuous broadening of the distributions of both $\langle l \rangle$ and $\langle d_{ee}/l \rangle$, indicated by the vertical bars in Fig. 3, represent a significant feature of the disordering process which remains to be understood in detail.

B. Disordering of minority stripe phase invading homogeneously magnetized initial state

We turn next to the description of the evolution of "banded" labyrinths, generated by the extensional growth of a single (or a few) stripe(s) of minority component nucleated from a homogeneous initial state in the course of demagnetization. By definition, demagnetization implies a decrease in value (from 1 to 0) of the parameter

$$m \equiv (M^{\uparrow}-M^{\downarrow})/(M^{\uparrow}+M^{\downarrow})$$

as the magnetic field is ramped from $H>H_{\mathrm{sat}}$ to $H=0$. Thus, an increasing amount of minority phase is being generated via the extensional growth of individual stripe domains. In the course of the elongation, the stripe width also increases in the manner shown in Fig. 1 of I: The width is identical to $d_{\downarrow}(H)$; the magnetic-field dependence of this quantity is given in that figure.

The process of stripe elongation is reversible, that is, the retraction of a meandering stripe may be accomplished by magnetizing a given film. This process entails the "dilution" of the minority component of magnetization while increasing the stripe period and represents an interesting analog to the "swelling" of lamellar surfactant assemblies [24].

Before elaborating on the evolution of patterns, we first note that the very nucleation of stripes from a state of saturated magnetization is at variance with the mean-field description of the phase behavior, discussed in I: Demagnetization of a saturated initial state should, according to that picture and the phase diagram depicted in Fig. 1 of I, lead to the nucleation of a hexagonal bubble lattice. As will be discussed elsewhere [35], bubble nucleation is indeed observed under certain conditions of demagnetizing, provided that $T \gtrsim 0.98T_c$. Otherwise, the scenario depicted in Fig. 4 unfolds: Individual sites of heterogeneous nucleation become the origin of an (eventually) "infinitely" elongated, meandering stripe domain of minority phase. The growth of such stripes appears to

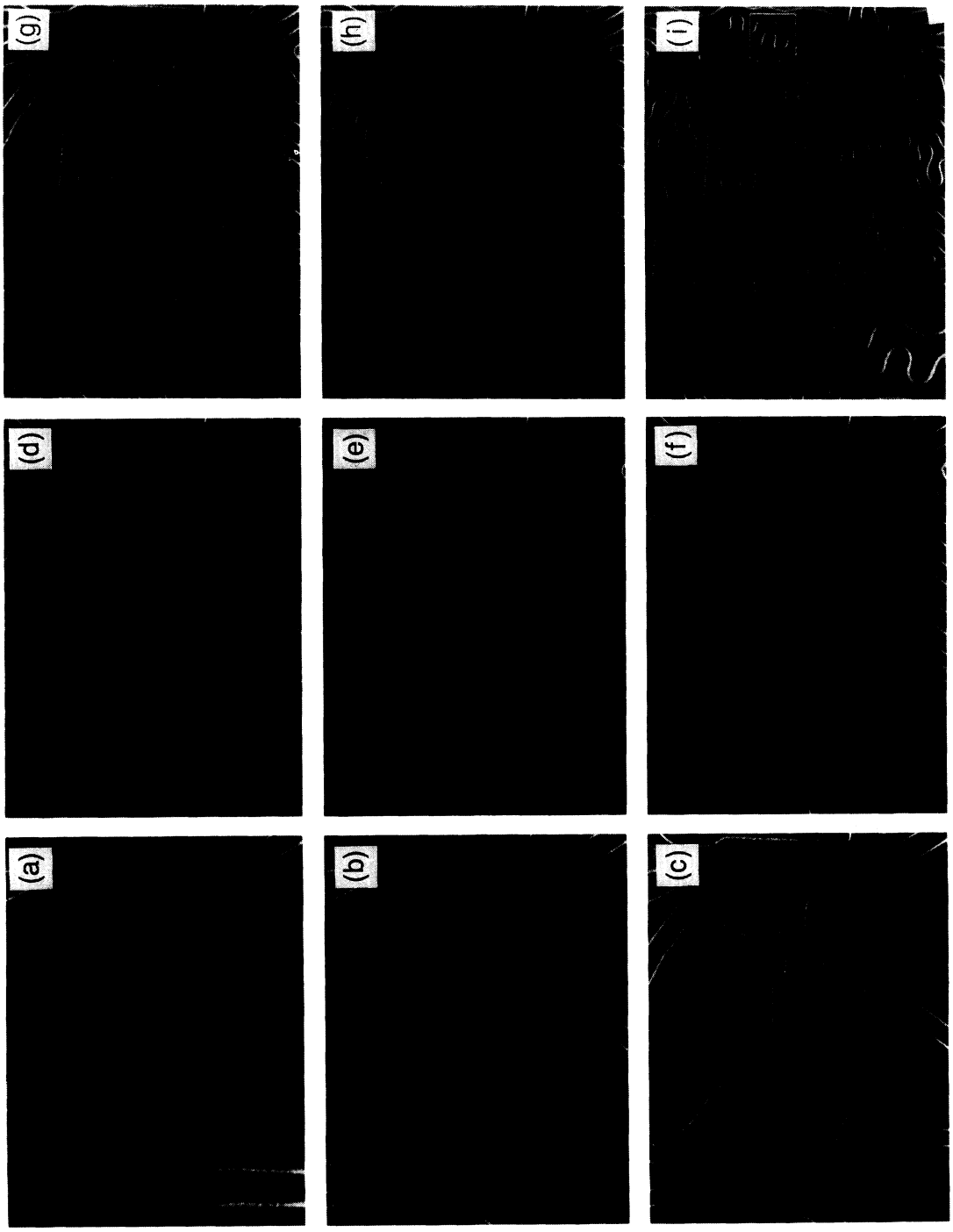

FIG. 4. Snapshots depicting intermediate states in the initial stage of the evolution of a banded labyrinth pattern at a temperature $T=160\,^{\circ}\mathrm{C}$ ($\simeq 0.8\,T_c$) from a homogeneously magnetized initial state (shown in black). Cascades of hairpins are triggered by a decrease in applied magnetic field in steps of approximately 1 Oe from an initial value of 70 Oe. Nucleation of stripes is first observed at $H=67$ Oe (a). (a)–(e) depict snapshots spaced, respectively, at time intervals of $\frac{1}{30}$ s, following nucleation. A second stripe nucleates from a spot approximately on the horizontal center line, on the right-hand side of the image in (b), and executes longitudinal switchbacks. Formation of transverse hairpins is particularly clearly visible in (b)–(e). (f) and (g) show the response to the next step in the field (to $H=66$ Oe) within two $\frac{1}{30}$-s time steps. (h) and (i) record the response to setting the field to $H=65$ Oe, the latter snapshot after a 1-s delay. The insets in the respective lower left corners of (a) and (i) contain a magnified rendition of the area highlighted in the originals, demonstrating that both interstripe spacing and stripe thickness remain unchanged in the course of the process shown here. The horizontal field of view of each panel is 1.4 mm.

preempt nucleation of additional domains.

The evolution of a well-defined local structure in the banded labyrinth requires the correct "folding" of a single (or generally a small number of) meandering stripe domain(s) to replicate the well-defined structural attributes of a labyrinthine pattern, as detailed in related articles [23,30]. Remarkably, this is accomplished at elevated temperatures without introducing a single topological defect in the evolving pattern, as we will presently discuss in connection with Figs. 4 and 5. We have previously pointed out the completely asymmetric distribution of topological defects between minority and majority components of the banded labyrinth pattern [23,30]. This broken symmetry distinguishes "banded" from "branched" labyrinths, such as those in Fig. 2, and reflects the history of pattern preparation involving, in this case, a distinct minority component.

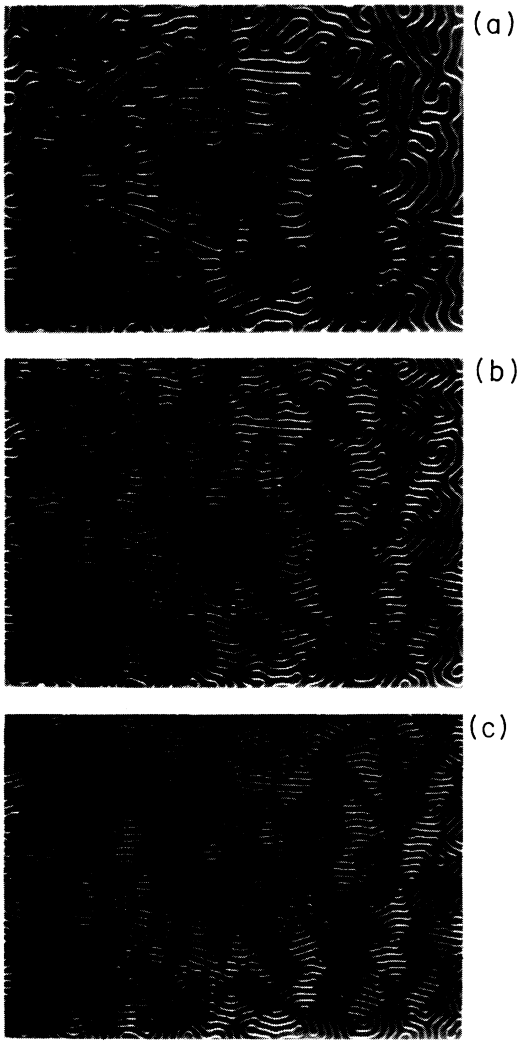

FIG. 5. Snapshots depicting intermediate states in the second stage of the evolution of a banded labyrinth pattern at a temperature $T=160\,^{\circ}\mathrm{C}$ ($\simeq 0.8T_c$) from a homogeneously magnetized initial state (shown in black). The initial stage of evolution is discussed in the text in connection with Fig. 4. The fully formed pattern "contracts" in response to the external field decreasing from 62 Oe (a) to 60 Oe (b) and 55 Oe (c). The respective stripe periods, in units of the period, $d=11.5$ μm of the final banded labyrinth state ($H=0$ Oe), are $3.2d$ (a), $2.9d$ (b), and $2.0d$ (c). The pattern topology is essentially fixed, remaining unaltered while the field is lowered to 0 Oe. During this process, disclinations, completely confined to the majority component, continue to unbind.

We now show that the evolution of banded labyrinths involves a distinct initial stage, required precisely for the reason that, immediately following minority stripe nucleation, large-scale spatial inhomogeneities exist in the evolving pattern. A sequence of snapshots documenting this initial stage in the evolution of a banded labyrinth pattern is displayed in Fig. 4.

As may be ascertained from this sequence of configurations, the growth of individual stripes is characterized by the formation of hairpin turns or loops. These are formed in two ways: first, by individual elongating stripes switching back on themselves and, second, by transverse protrusions from individual stripes, originating predominantly near spontaneously formed "bulges" (see Fig. 4) in the parent stripe and extending into pristine regions of majority component. Following small stepwise changes in the applied field, cascades of hairpin-loop formation are triggered which require frame-by-frame resolution ($\frac{1}{30}$ s) to track. Remarkably, the (normal) distance between the legs even of isolated hairpins [see, e.g., Figs. 4(a)–4(c)] is very well defined and appears to be identical to the period of the stripe pattern which first realizes a (very nearly) homogeneous coverage of the available sample area with minority component, as may be ascertained from the comparison of Figs. 4(a) and 4(i), and their respective insets. It is when this homogeneous state is attained that large lateral gradients in the strain are eliminated, signaling termination of the initial stage of evolution. As may be judged from Figs. 4(a)–4(i), the stripe width remains essentially unchanged during this first stage; referring to Fig. 1 of I, this is a direct indication that the process of eliminating lateral inhomogeneities is complete within a very small interval of applied field following nucleation (see also the caption of Fig. 4). Stated differently, the initial stage of evolution of banded labyrinth patterns eliminates large inhomogeneities in the distribution of minority component within the background of the majority component, thereby eliminating lateral gradients in the strain. During this evolution, a crossover occurs from single stripe to collective stripe properties: an area-filling pattern with a period, well defined over the available sample area, emerges at the completion of the initial stage of evolution. The nature of this crossover and the behavior of the single stripe, especially the mechanism driving hairpin formation, are not presently understood.

As Fig. 4 reveals, essential topological features of the ultimately attained banded labyrinth are determined at this very early stage of the evolution. In particular, the density of disclinations, all in the *majority* component, is essentially fixed, and given by the number of hairpin turns of the meandering stripe of invading *minority* component. That is, elongating stripe domains, by generating the appropriate density and distribution of hairpins, very remarkably, replicate the morphology of the branched la-

byrinthine pattern by "folding" into the correct local structure.

In the course of the ensuing second stage of the pattern evolution, illustrated in Fig. 5, the now completely formed stripe pattern responds to the decreasing applied field by "contracting," i.e., by decreasing its modulation period. The overall configuration, however, is essentially fixed and undergoes, if any, only minor local rearrangements. Further analysis in fact shows that this second stage of the evolution is mediated by the elongation of already unbound pairs of disclinations, present in the majority component, in a manner identical to that mediating the evolution of the branched labyrinth patterns, as discussed in Sec. III A and in I.

A crucial aspect of the late stage of the disordering process is the necessity to accommodate the local compression of the evolving stripe pattern, implied by the field-induced decrease of the characteristic period apparent in Fig. 5. The requisite adjustment involves the motion of domain walls transverse to the locally prevailing stripe orientation. A lag in the response of the pattern with respect to the rate of change of magnetic field—for example, due to domain-wall pinning—implies the accumulation of local strain. Given a finite mobility of domain walls [39] and a sufficiently rapid rate of demagnetization, local strain may exceed the threshold for nucleation of disclination dipoles. This is precisely the scenario setting the stage for the proliferation of defects and line-branching events characterizing a new class of metastable patterns to whose description we turn next.

C. Kinetic effects: Disclination unbinding versus nucleation

The evolution of the branched and banded labyrinthine states we have described in Secs. III A and III B originates in very different initial states and involves distinct mechanisms: In the first case, the "smectic" instabilities of an ordered state and the formation and subsequent unbinding of disclination dipoles and, in the second case, the hairpin folding of individual stripes of minority component, a process delineating disclination dipoles in the majority component, and the subsequent unbinding of these defects. Quite surprisingly in view of these differences in the respective processes of generating the final, disordered state, the local structural attributes and characteristic motifs of both types of labyrinthine patterns were demonstrated to be virtually identical and reproducible. Common to the preparation of both these patterns is a choice of conditions permitting the rapid equilibration of strain in response to changes in external parameters, i.e., temperature and magnetic field—that is, "adiabatic" conditions prevail. This prevents the buildup of significant local gradients in the strain field.

In contrast, magnetic-field-induced strain in an evolving pattern may be increased sufficiently rapidly, particularly in the low-temperature region of the phase diagram where domain-wall mobility is decreased, so that a new class of metastable patterns is produced. An essential distinction between patterns representative of this new type and the former branched and banded labyrinth patterns becomes apparent when inspecting Fig. 6: This new class of pattern, described as "comblike" when first reported [40], exhibits a very high density of topological defects, generally in the form of chains of interdigitating disclination dipoles. The new type of patter displays none of the local structural attributes identified and analyzed in the case of both branched and banded labyrinths [30]—in particular, there are no oblong polygonal segment clusters.

In contrast to the asymmetry in the distribution of to-

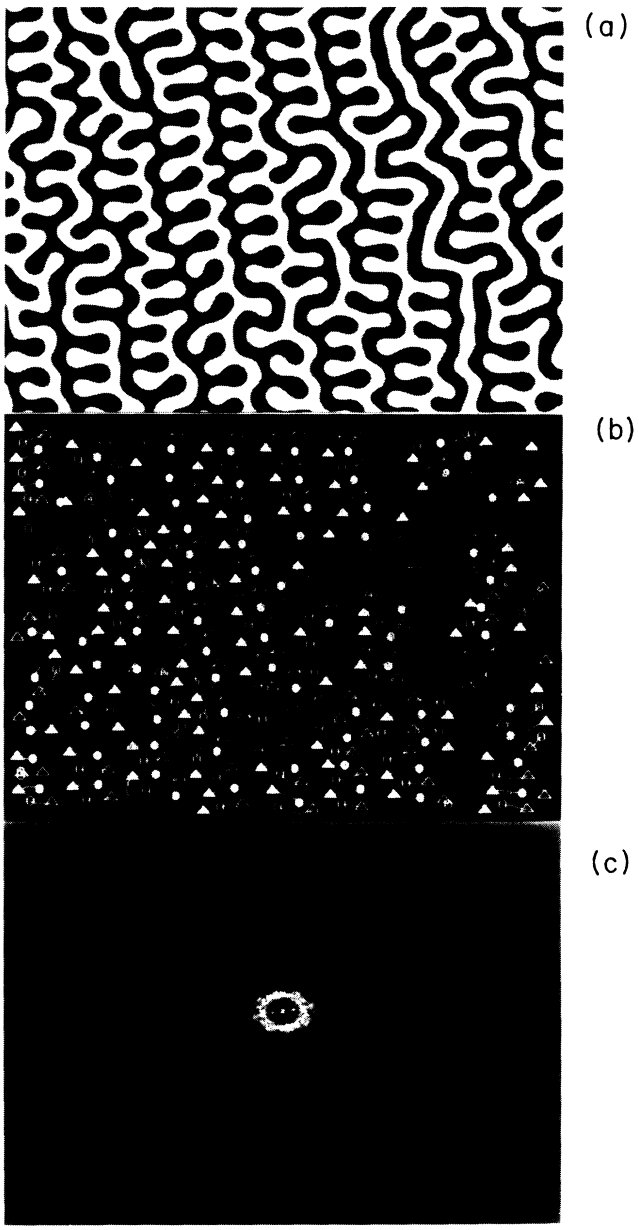

FIG. 6. "Comb" pattern, generated at room temperature by rapid demagnetization from a saturated state. This type of pattern is characterized by an unusually high density of line-branching events and hence disclinations; these are paired into dipoles which interdigitate and form linear chains. (a) (top) depicts the pattern itself, (b) (middle) depicts its topological defects and connecting tethers identified by a set of algorithms for line-pattern analysis [30]. The horizontal dimension of the field of view is 570 μm. (c) (bottom) contains the Fourier spectrum computed from the pattern in (a).

pological defects with respect to the pattern components in the banded labyrinths obtained by demagnetization at elevated temperatures, defects are now present in virtually equal numbers in both components. In addition, a preferred orientation is retained over macroscopic distances, yielding Fourier spectra exhibiting basically fourfold symmetry as illustrated in Fig. 6(c). The dipole chain morphology is reminiscent of that previously encountered as an intermediate in the transformation of a chevron to a branched labyrinth and described in connection with Fig. 10 of I. These two observations may indicate that the initial stage of pattern evolution involves the generation of a quasilamellar pattern. However, it has so far been impossible to achieve the requisite time resolution to track the evolution of "comb" patterns.

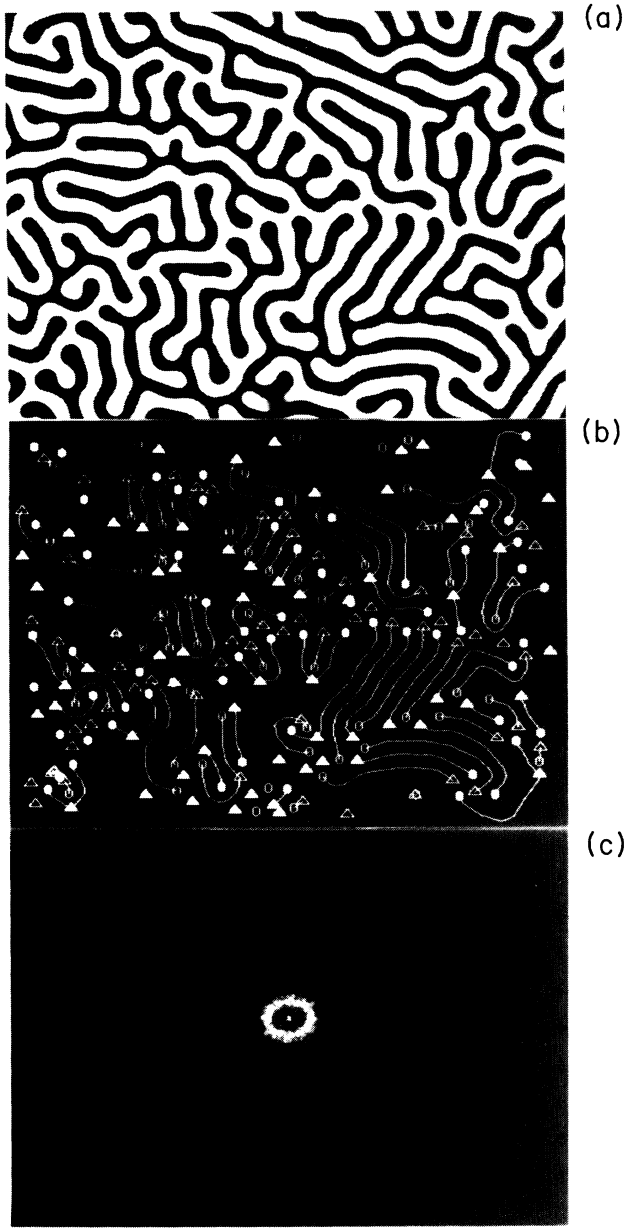

FIG. 7. Coexistence of "comb" and branched labyrinth morphologies in stripe patterns, generated by rapid demagnetization from saturation at room temperature under conditions discussed in Sec. III C of the text. (a) (top) depicts the pattern itself, and (b) (middle) its topological defects and connecting tethers, identified by a set of algorithms for line-pattern analysis [30]. The horizontal dimension of the field of view is 570 μm. (c) (bottom) contains the Fourier spectrum computed from the pattern in (a).

The density of defects is exceptionally high, exceeding that typical of branched and banded labyrinths by a factor of 5 or more in the cases we have analyzed. Importantly, in the present patterns dipoles remain essentially intact even in the final state. A typical value for $\langle d_{ee}/l \rangle$, obtained for the pattern in Fig. 6, is 0.94. We also note that the density of defects and the average tether contour length are correlated so that, approximately, $n_D \langle l \rangle \simeq$ const. We are led to conclude that the process of disclination-dipole unbinding has been suppressed in favor of continued defect nucleation: The result is a highly branched, essentially lamellar pattern of *incorrect* spacing, spawning interlocking sidebranches to achieve the correct local periodicity.

The emergence of the highly branched comb patterns with the striking ordered superstructure of chains of interdigitated disclination dipoles is unusual. We have observed it most frequently in "new" samples, believed to be free of imperfections and thus expected to display a uniformly low coercivity. More typical under very similar experimental conditions, namely, rapid demagnetization at room temperature, is the observation of patterns such as that of Fig. 7. In terms of the structural attributes we have employed to analyze labyrinthine patterns, metastable patterns such as the one in Fig. 7 may be viewed as being composed of coexisting regions of comb and branched labyrinth patterns. For example, the density of disclination pairs and the mean values for $\langle l \rangle \simeq 58$ and $\langle d_{ee}/l \rangle \simeq 0.86$ are all intermediate between those of branched and banded labyrinths, on the one hand, and the comb pattern, on the other. Moreover, the pattern of Fig. 7 is seen to contain the structural motifs of both types of pattern. That is, chains of interdigitating disclination dipoles coexist with segment clusters: In regions exhibiting the former morphology, the defect density is high, while tether contours are short; in regions exhibiting the latter morphology, a smaller number of elongating or unbinding disclination dipoles emerge.

Within the context of attributing the proliferation of disclination dipoles to gradients in the strain field and local accumulation of strain, in turn reflecting limits in the mobility of domain walls, one must conclude that the coexistence of different types of pattern morphologies indicates inhomogeneities in domain-wall mobility, perhaps due to an inhomogeneous distribution of pinning sites.

IV. DISCUSSION

In Sec. III and in I we have addressed the evolution of disordered stripe-domain states in ferrimagnetic garnet films. This process, mediated by temperature- or field-induced strain, enables the selection of a stripe pattern of globally correct period, $d = d(H,T)$. In general, this period adjustment is not possible while maintaining the

lamellar stripe configuration of globally minimal free energy; consequently, disordered patterns appear. The pattern morphology represents the optimal realization of a stripe phase of correct period under a set of additional constraints which eliminate the lamellar pattern. For the garnets studied here, such a constraint generally arises in the form of suppressed nucleation of additional lamellae. That is, the actual number of stripes N_L is incorrect: $N_L < L_0/d$, L_0 denoting the linear sample dimension. As a result, the available area $A_0 \simeq L_0^2$ must be filled with a stripe pattern of minimal free energy which exhibits the required period d as well as the correct stripe width, or equivalently, produces the correct magnetization m.

We have characterized the process of disordering by explicitly focusing on topological point defects—notably, disclinations. Two mechanisms of introducing disorder into a given pattern were distinguished, namely, the proliferation of defect pairs by continued nucleation and the topologically constrained "unbinding" of disclination dipoles whose constituent charges remain linked by a well-defined "tether." Different pattern morphologies emerge depending on which of the two processes is favored. Under most conditions, disclination-pair unbinding predominates over nucleation of additional defects. That is, the elongation of existing stripes, accompanied by the loss of orientational order, takes precedence over stripe branching, a mechanism by which additional lines may be injected into an existing pattern. Strong topological constraints govern this process; in particular, rupture and self-intersection of evolving stripes or tethers are forbidden. These constraints severely restrict the range of accessible configurations of labyinthine stripe pattern: In fact, its morphological properties turn out to be statistically robust [30] and lamellar ordering is realized locally within "cybotactic" segment clusters.

An extreme case of extensional growth is encountered in the evolution of banded labyrinth patterns, mediated by the formation of hairpins during longitudinal as well as transverse elongation of one (or a few) individual stripe(s) occurring without a single branching event. Here, one generates a pattern of predetermined d and $m=0$ from an initial state without domain structure, characterized by $m=1$. In the absence of a domain pattern, no stripe period is defined: Consequently, the period itself has to emerge during pattern evolution, and we have shown that this occurs during an initial stage characterized by cascades of hairpin formation, as documented in Fig. 4.

There is currently no explanation for the occurrence of the ostensibly spontaneous 180° reversals of the growth direction of individual stripe domains, nor for the formation of hairpins in the form of transverse protrusions in the early stages of elongation. In fact, the assumption inherent in the mean-field picture of Garel and Doniach [8] is that the interaction between adjacent stripes of equal magnetization and hence the self-interaction of a stripe executing a hairpin loop are repulsive. On the other hand, Tsebers and Maiorov [11] have carried out a linear stability analysis of the free-energy functional governing the shapes of individual cylindrical and stripe domains in thin layers of ferrofluid, closely related to the system at hand. The analysis reveals that the linear configuration of a single stripe domain of length L is unstable with respect to bending into U (horseshoe or hairpin) and S shapes, with corresponding unstable modes $2\pi/L$ and π/L, respectively. An instability of large amplitude, presumably governed by an effective bending stiffness, might indeed produce a U-shaped configuration.

However, one may also wonder whether the formation of hairpin turns is favored by additional magnetic interactions between domain walls involving intralayer components of the magnetization, not considered in the original Garel-Doniach treatment. Whatever the direction chosen by the very first stripe invading a pristine region of majority component, it appears that this breaks azimuthal symmetry locally, defining a preferred orientation for successive portions of stripe. A situation somewhat reminiscent in terms of the prevailing hairpin morphology is encountered in nematic liquid-crystal polymers where hairpins arise from the competition of nematic alignment of the polymer chain and its configurational entropy [41]. In contrast to the global symmetry-breaking inherent in the nematic ordering, however, there is no such preferred direction in our patterns which are in fact globally disordered.

The mode of pattern evolution leading to banded labyrinths may be viewed as a "space-filling," self-avoiding walk. Simulations were undertaken on a square lattice to assess the effect on the configuration of the walk of imposing *local* constraints. Thus, the probability of turns taken by the growing ends of a stripe was biased such that the greatest weight was given to continuation in the forward direction and turns by more than $\pm\pi/2$ were forbidden; in addition, self-avoidance was *locally* enforced. These simulations [42] lead to rapid self-trapping of growing stripes and produce irregular shapes, clearly demonstrating that local constraints are insufficient to generate the "cybotactic" segment clusters of parallel line segments characterizing banded labyrinth patterns [23,30]. Recent Monte Carlo simulations employing the full, nonlocal repulsive interaction of the Garel-Doniach Hamiltonian have been successful in generating typical labyrinthine stripe morphologies of the type observed here [43]. It would be of interest to replicate the peculiar evolution of banded labyrinths and to determine how the characteristic density and spatial distribution of hairpins arise.

A pattern of identical features also evolves from a lamellar initial state, characterized by a given $d=d(T_0)=d_0$ and $m=0$ upon heating along the $H=0$ symmetry axis in the mean-field phase diagram. In contrast to the predominating nonlocal interactions governing the initial stage of evolution of banded labyrinths, the smectic elastic response of the ordered lamellar state to the accumulation of dilative strain appears to be well accounted for by a local theory. These lamellar instabilities lead to undulation and chevron patterns, exhibiting, respectively, curvature and discontinuity walls. The chevron pattern eventually becomes unstable with respect to the formation of disclination dipoles in which a characteristic number of line-branching events serve as a mechanism of nucleating additional lamellae. The subsequent

topologically constrained disclination-dipole unbinding also constitutes a form of elongation. The final disordered state represents a realization of a "branched" labyrinthine pattern. The same topological constraints as those encountered before govern the process of formation of branched labyrinths, ensuring that evolving lines do not break and do not self-intersect.

Since the analysis of morphological and structural attributes reveals the identity of banded and branched labyrinths from a statistical structural point of view, we are led to conclude that the elongation of existing lines under the operative topological constraints produces a well-defined final state corresponding to the constrained minimization of a suitable free-energy functional. The labyrinthine patterns exhibit many of the structural features generally associated with amorphous structure, discussed in Sec. III of I. In particular, they contain a network of disclinations and retain the structure of the ordered state, in this case lamellar stripe configurations, over some intermediate distance scale.

There remains the challenge of providing a detailed understanding of the robust local structural attributes, and characteristic defect density of the labyrinthine patterns. It is conceivable that a model of constrained optimization, implemented in the form of space-filling walks, may provide a useful approach, particularly for computer simulation. Another possibility, suggested by Huse [44], might be to consider the configuration of the network formed by segment cluster boundaries [30].

Under experimental conditions favoring the rapid accumulation of local dilative strain, proliferation of disclination dipoles is favored over dipole unbinding. In that case, highly branched patterns emerge in which (imperfectly) ordered linear arrays of interdigitated disclination dipoles constitute the predominant motif. The preservation of preferred orientations and the spontaneous formation of defect arrays suggest a collective process. The defect density in these comb patterns is so high as to preempt disclination-dipole unbinding; it appears that it is this latter process which must occur to destroy global orientational order in the pattern.

The pattern morphology permits an unequivocal distinction between the kinetically favored, highly branched and the fully evolved labyrinthine patterns. Invoking our suggestion that it is a lag in the (transverse) motion of domain walls which permits the accumulation of local strain and thus favors defect nucleation, we may say that a macroscopic record exists, in form of the pattern morphology, of the distribution of microscopic material properties, such as pinning sites.

It is interesting to speculate about a similar relationship between line branching, that is, defect proliferation, in the stripe pattern and microscopic domain-wall structure—specifically, vertical Bloch lines. These are topological defects, considered to hold promise for future technological applications [45]. They are found along Bloch domain walls and result from chiral symmetry breaking: The transverse component of magnetization in the center of a Bloch wall displays opposite signs on either side of such a defect. A connection of this nature between macroscopic pattern features and microscopic structure was surmised in the initial report of comb patterns and may represent a subject for fruitful further investigation; direct imaging of vertical Bloch lines looks particularly promising [45].

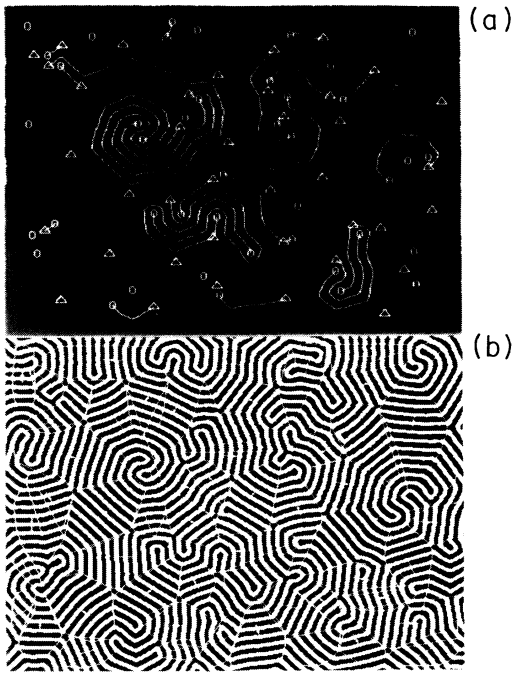

FIG. 8. Interlocking spirals, illustrated in the upper left quadrant of (a) (top), are frequently observed in branched labyrinths. They give rise to a "rosette" structure in the pattern morphology, exemplified by (b) (bottom): "Segment clusters" share the core of the spiral as a common vertex [23,30]; the left portion of another rosette structure is visible near the right-hand edge of the figure. These structural features are very prominent in color-coded images [23]. The horizontal dimension of the field of view is 570 μm.

Events analogous to line branching are also observed in other physical systems exhibiting modulated phases, specifically in ferrofluid [12,13] and amphiphilic monomolecular (Langmuir) films [17]. As with magnetic garnets, the kinetics governing local domain-wall motion is crucial, especially in the aforementioned systems whose order parameter is conserved. For example, the shape instability transforming an individual distorted circular domain in a Langmuir film into a stripe [6] produces different morphologies under rapid and slow tuning of the relevant parameter, in this case the compression of a film of fixed composition, confined to an air-water interface. Rapid compression leads to what we have in fact previously referred to as a "branching" instability of a given domain [17] while a very slow approach to threshold, permitting intralayer transport to mediate the requisite deformation of the domain boundary, does indeed lead to elongation of the domain and the suppression of branching [46]. We expect the analogous situation for ferrofluid films.

As we have pointed out, the disordered patterns analyzed here may be considered metastable states, selected as a result of the minimization of a suitable free-energy functional in the presence of topological constraints. In

particular, the absence of line breaking ensures the global connectivity of the pattern. Consequently, one would certainly expect resistance to shear: The disordering considered here is thus not equivalent to melting.

In the case of the branched labyrinth, the topological connectivity of the labyrinthine patterns in the absence of line breaking and line crossing constitutes a property that guarantees a well-defined relationship between the final, disordered and the initial, ordered state: the disordered system will retrace its path through phase space and recover the original representation of the ordered phase if the external strain-inducing parameter is reversed. In fact, one might argue that it is the very absence of line breaking which precludes the occurrence of a phase transition: Only if such a process were permitted would topological constraints be released and the appearance of line "ends," or free $+\frac{1}{2}$ disclinations, be ensured. Particularly suggestive in this context are regions, frequently formed in the course of disclination-dipole unbinding and illustrated in Fig. 8, in which two counterpropagating, elongating lines "wind up" into two interlocking spirals; such regions are decorated by segment clusters sharing the core of the spirals as a common vertex in a "rosette" conformation, as illustrated in Fig. 8(b). Line breaking appears to offer the only mechanism to release the wound-up phase of the order parameter and so ensure the vanishing of the shear response [47].

From these considerations it would seem that the possibility of observing true stripe-phase melting in two dimensions requires the existence of events including spontaneous line breaking and the implied proliferation of free disclinations. Such a situation may exist in magnetic garnets near the critical temperature, an issue currently under investigation in connection with ongoing experiments addressing the experimental phase behavior of these films [35]. Thermal fluctuations of the type of interest, inducing line breaking, are readily observable in a binary amphiphilic monomolecular film where a transition between an ordered stripe phase of twofold rotation symmetry and a stripe liquid has been very recently observed [18].

ACKNOWLEDGMENTS

L. Monar's technical contributions in constructing experimental apparatus are gratefully acknowledged. Various aspects of the work described here have benefited from a number of useful conversations with E. Bodenschatz, S. Hudson, D. Huse, D. Nelson, L. O'Gorman, and S. Singer.

[1] T. Mitsui and J. Furuichi, Phys. Rev. **90**, 193 (1953).
[2] T. F. Faber, Proc. R. Soc. London Ser. A **248**, 460 (1958).
[3] R. Rosensweig, *Ferrohydrodynamics* (Cambridge University Press, Cambridge, 1982), Chap. 7.
[4] C. Kittel, Phys. Rev. **70**, 965 (1946); Rev. Mod. Phys. **21**, 541 (1949).
[5] C. Kooy and U. Enz, Philips Res. Rep. **15**, 7 (1960).
[6] H. M. McConnell, Annu. Rev. Phys. Chem. **42**, 171 (1991).
[7] D. Andelman, F. Brochard, and J.-F. Joanny, J. Chem. Phys. **86**, 3673 (1987).
[8] T. Garel and S. Doniach, Phys. Rev. B **26**, 325 (1982).
[9] J. A. Cape and G. W. Lehman, J. Appl. Phys. **42**, 5732 (1971).
[10] I. B. Puchalska, G. A. Jones, and H. Jouve, J. Phys. D **11**, L175 (1978).
[11] A. O. Tsebers and M. M. Maiorov, Magnetohydrodyn. **16**, 21 (1980).
[12] R. E. Rosensweig, M. Zahn, and R. J. Shumovich, J. Magn. Magn. Mater. **39**, 127 (1983).
[13] S. A. Langer, R. E. Goldstein, and D. P. Jackson (unpublished).
[14] P. Molho, J. L. Porteseil, Y. Souche, J. Gouzerh, and J. C. S. Levy, J. Appl. Phys. **61**, 4188 (1987).
[15] P. Molho, J. L. Porteseil, and Y. Souche, J. Appl. Phys. **63**, 4327 (1988).
[16] R. Seshadri and R. M. Westervelt, Phys. Rev. Lett. **66**, 2774 (1991).
[17] M. Seul and M. J. Sammon, Phys. Rev. Lett. **64**, 1903 (1990); M. Seul, Physica A **168**, 198 (1990).
[18] M. Seul and V. S. Chen (unpublished).
[19] J. Toner and D. R. Nelson, Phys. Rev. B **23**, 316 (1981).
[20] D. R. Nelson and J. Toner, Phys. Rev. B **24**, 363 (1981).
[21] D. R. Nelson, Phys. Rev. B **26**, 269 (1982).
[22] M. Seul and R. Wolfe, Phys. Rev. Lett. **68**, 2460 (1992).
[23] M. Seul, L. R. Monar, L. O'Gorman, and R. Wolfe, Science **254**, 1616 (1991).
[24] D. Sornette, J. Phys. (Paris) **48**, 151 (1987); **48**, 1413 (1987).
[25] N. A. Clark and R. B. Meyer, Appl. Phys. Lett. **22**, 493 (1973); R. Ribotta and G. Durand, J. Phys. (Paris) **38**, 179 (1977).
[26] Ch. S. Rosenblatt, R. Pindak, N. A. Clark, and R. B. Meyer, J. Phys. (Paris) **38**, 1105 (1977); N. A. Clark and A. J. Hurd, *ibid.* **43**, 1159 (1982).
[27] J. M. Kosterlitz and D. J. Thouless, J. Phys. C **6**, 181 (1973).
[28] K. J. Strandburg, Rev. Mod. Phys. **60**, 161 (1988).
[29] S. Ostlund and B. I. Halperin, Phys. Rev. B **23**, 335 (1981).
[30] M. Seul, L. R. Monar, and L. O'Gorman, Philos. Mag. B **66**, 471 (1992).
[31] L. Landau and E. M. Lifshitz, *Electrodynamics of Continuous Media* (Pergamon, New York, 1959), Vol. VIII, Chap. 39.
[32] S. Inoué, *Video Microscopy* (Plenum, New York, 1987).
[33] E. W. Hansen, J. A. Conchello, and R. D. Allen, J. Opt. Soc. Am. A **5**, 1836 (1988).
[34] M. Seul, M. J. Sammon, and L. R. Monar, Rev. Sci. Instrum. **62**, 784 (1991).
[35] M. Seul and R. Wolfe (unpublished).
[36] J. Rudnick and G. Gaspari, Science **237**, 384 (1987).
[37] P. J. Flory, *Statistical Mechanics of Chain Molecules* (Hanser, Munich, 1969).
[38] J. Des Cloiseaux and G. Jannink, *Polymers in Solution: Their Modeling and Structure* (Clarendon, Oxford, 1990).
[39] A. P. Malozemoff and J. C. Slonczewski, *Magnetic Domain Walls in Bubble Materials*, edited by R. Wolfe (Academic, New York, 1979).
[40] R. Wolfe and J. C. North, Bell Syst. Tech. J. **51**(6), 1436 (1972).
[41] J. M. F. Gunn and M. Warner, Phys. Rev. Lett. **58**, 393

(1987).
[42] M. Seul (unpublished); for a similar problem, see, e.g., J. W. Lyklema and K. Kremer, J. Phys. A **17**, L691 (1984).
[43] M. M. Hurley and S. J. Singer, J. Phys. Chem. **96**, 1938 (1992); **96**, 1951 (1992).
[44] D. Huse (private communication).
[45] A. Thiaville, J. Ben Youssef, Y. Nakatani and J. Miltat, J. Appl. Phys. **69**, 6090 (1991).
[46] M. Seul (unpublished).
[47] B. I. Halperin, in *Physics of Defects,* Les Houches, Session XXXV, 1980, edited by R. Balian *et al.* (North-Holland, Amsterdam, 1981), Chap. 14.

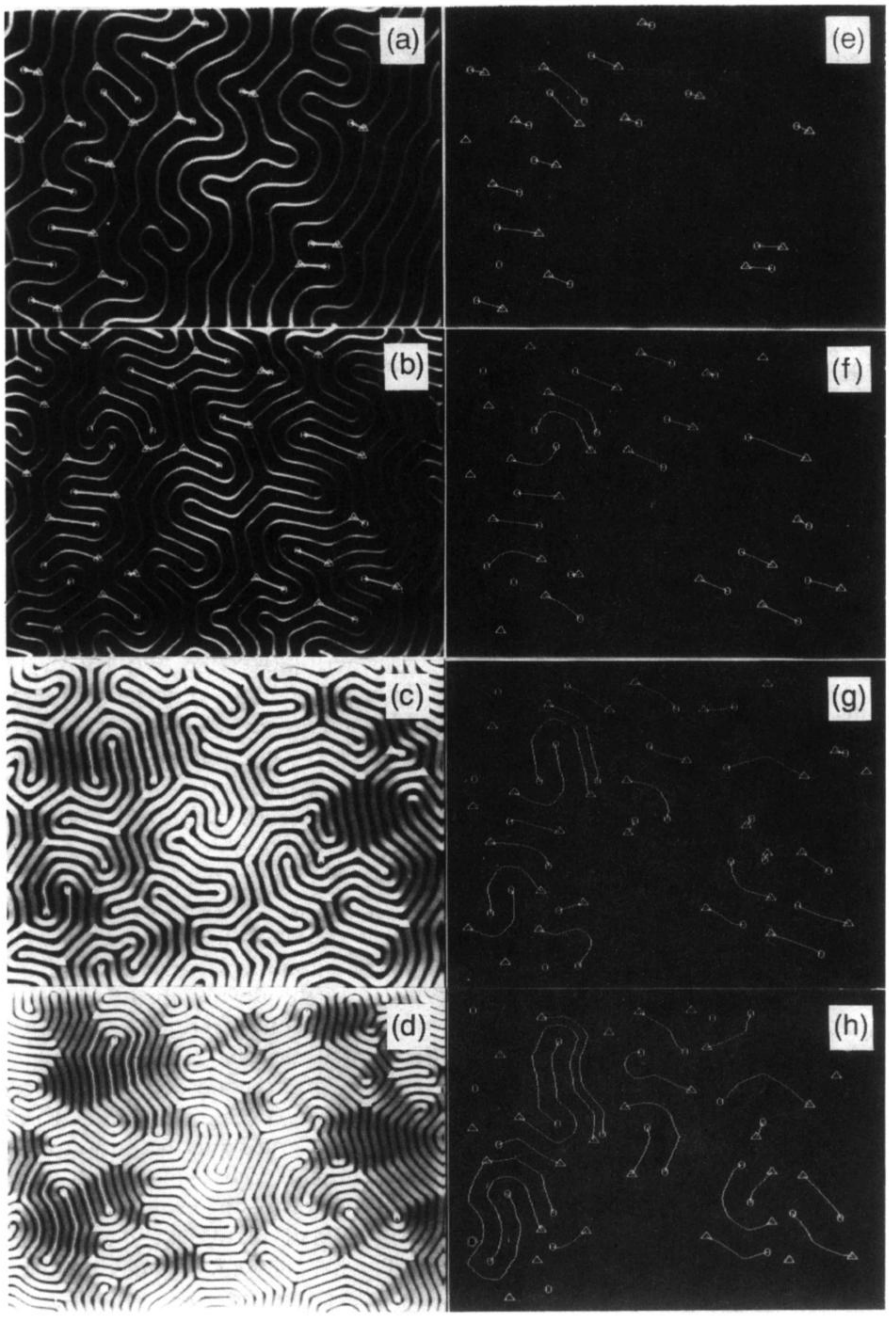

FIG. 2. Intermediate states in the course of disclination-dipole unbinding, formed in response to magnetic-field-induced dilative strain; $T=160\,^{\circ}\mathrm{C}$ ($\simeq 0.8T_c$). The bottom row depicts a branched labyrinth pattern at $H=0$ Oe. Preceding the pattern in the top row is a lamellar pattern, not shown here. The right-hand column contains $-\frac{1}{2}$ ("Δ") and $+\frac{1}{2}$ ("$\circ$") disclinations as well as the connecting tether, identified in the corresponding stripe pattern by a set of algorithms for line-pattern analysis [30]. In the left-hand column, disclination charges ("Δ," "$\circ$") and the connecting tethers are superimposed on the original stripe pattern [22]. The stripe patterns displayed in the two lower panels on the left were treated by application of low-pass and dilation filters. The shading so generated makes it readily apparent that disclinations are located along the boundaries of "segment" clusters, i.e., order regions composed of parallel stripe segments [23,30]. An analysis of this data set has been previously presented [22]. The horizontal dimension of each field of view is 570 μm.

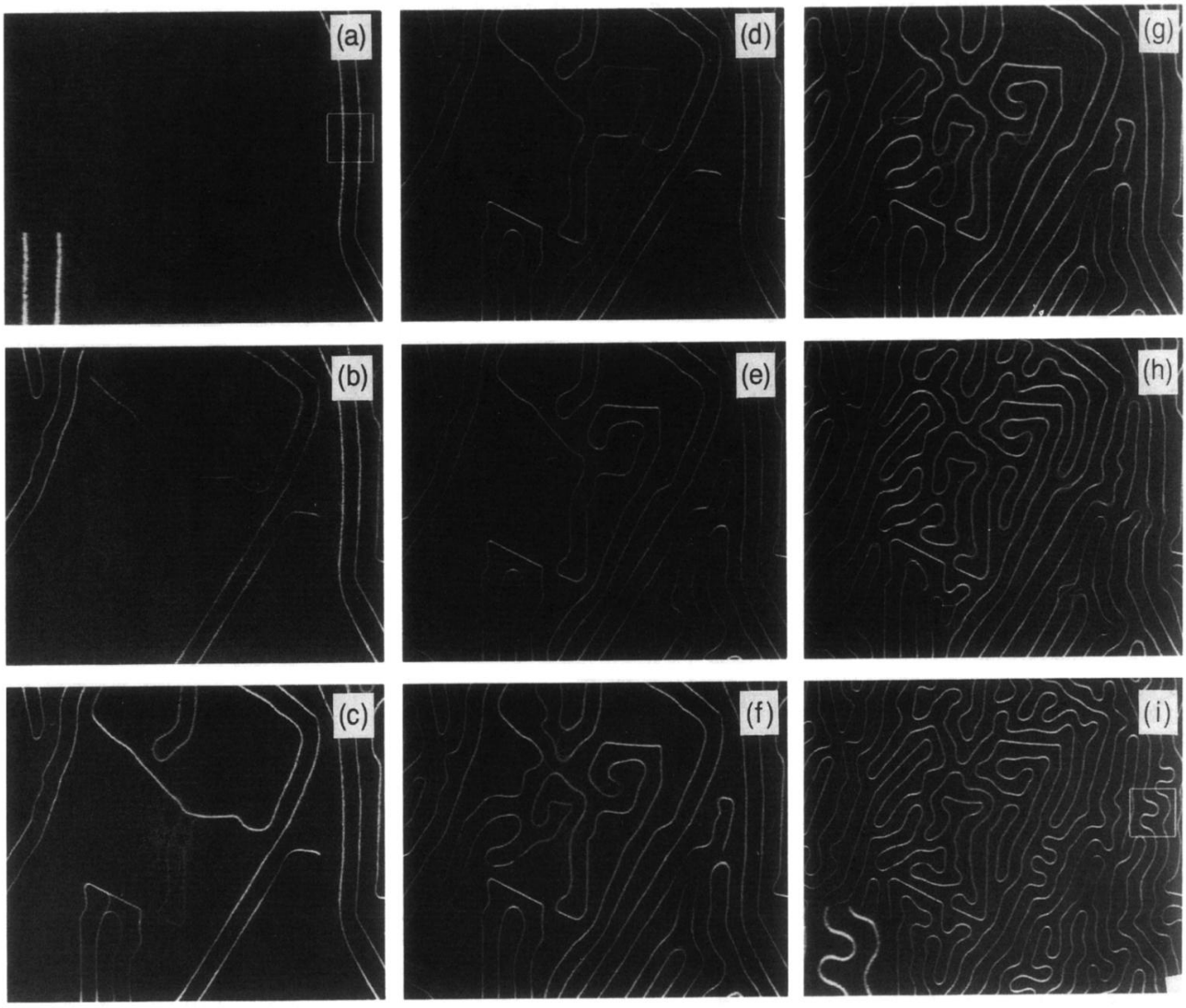

FIG. 4. Snapshots depicting intermediate states in the initial stage of the evolution of a banded labyrinth pattern at a temperature $T=160\,^{\circ}\mathrm{C}$ ($\simeq 0.8T_c$) from a homogeneously magnetized initial state (shown in black). Cascades of hairpins are triggered by a decrease in applied magnetic field in steps of approximately 1 Oe from an initial value of 70 Oe. Nucleation of stripes is first observed at $H=67$ Oe (a). (a)–(e) depict snapshots spaced, respectively, at time intervals of $\frac{1}{30}$ s, following nucleation. A second stripe nucleates from a spot approximately on the horizontal center line, on the right-hand side of the image in (b), and executes longitudinal switchbacks. Formation of transverse hairpins is particularly clearly visible in (b)–(e). (f) and (g) show the response to the next step in the field (to $H=66$ Oe) within two $\frac{1}{30}$-s time steps. (h) and (i) record the response to setting the field to $H=65$ Oe, the latter snapshot after a 1-s delay. The insets in the respective lower left corners of (a) and (i) contain a magnified rendition of the area highlighted in the originals, demonstrating that both interstripe spacing and stripe thickness remain unchanged in the course of the process shown here. The horizontal field of view of each panel is 1.4 mm.

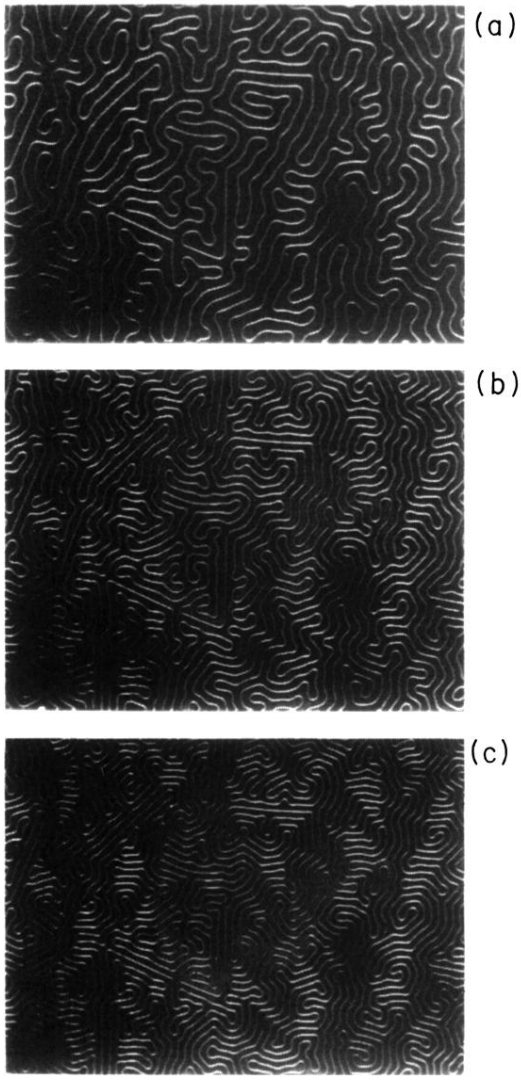

FIG. 5. Snapshots depicting intermediate states in the second stage of the evolution of a banded labyrinth pattern at a temperature $T=160$°C ($\simeq 0.8T_c$) from a homogeneously magnetized initial state (shown in black). The initial stage of evolution is discussed in the text in connection with Fig. 4. The fully formed pattern "contracts" in response to the external field decreasing from 62 Oe (a) to 60 Oe (b) and 55 Oe (c). The respective stripe periods, in units of the period, $d=11.5$ μm of the final banded labyrinth state ($H=0$ Oe), are $3.2d$ (a), $2.9d$ (b), and $2.0d$ (c). The pattern topology is essentially fixed, remaining unaltered while the field is lowered to 0 Oe. During this process, disclinations, completely confined to the majority component, continue to unbind.

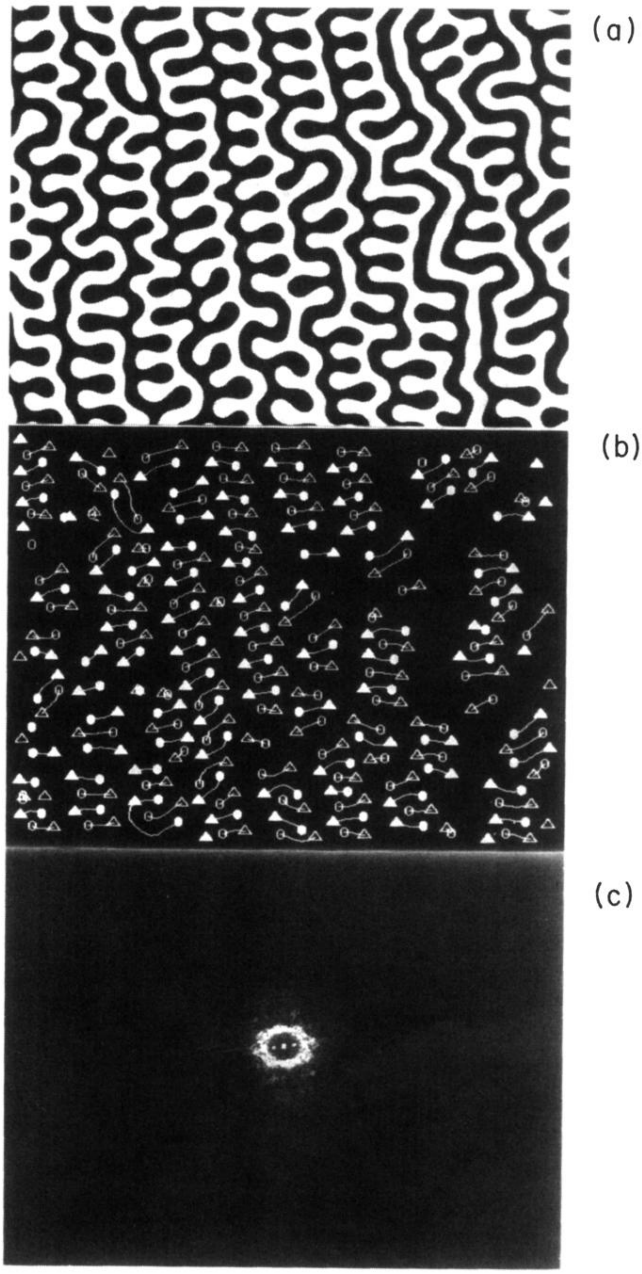

FIG. 6. "Comb" pattern, generated at room temperature by rapid demagnetization from a saturated state. This type of pattern is characterized by an unusually high density of line-branching events and hence disclinations; these are paired into dipoles which interdigitate and form linear chains. (a) (top) depicts the pattern itself, (b) (middle) depicts its topological defects and connecting tethers identified by a set of algorithms for line-pattern analysis [30]. The horizontal dimension of the field of view is 570 μm. (c) (bottom) contains the Fourier spectrum computed from the pattern in (a).

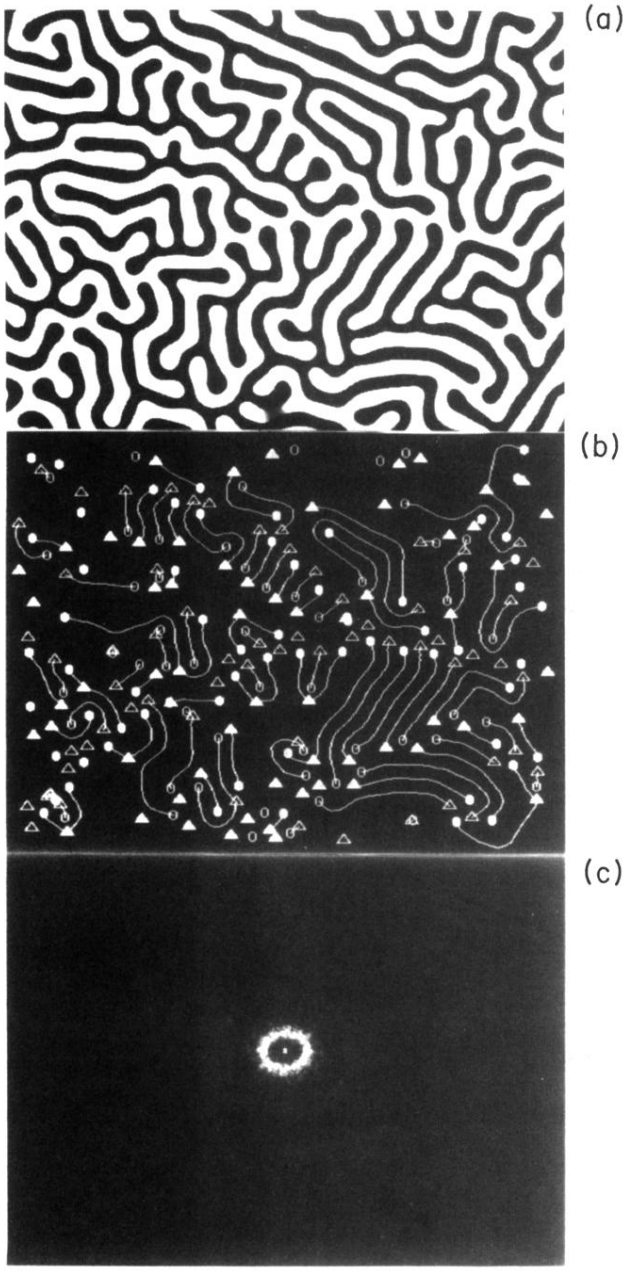

FIG. 7. Coexistence of "comb" and branched labyrinth morphologies in stripe patterns, generated by rapid demagnetization from saturation at room temperature under conditions discussed in Sec. III C of the text. (a) (top) depicts the pattern itself, and (b) (middle) its topological defects and connecting tethers, identified by a set of algorithms for line-pattern analysis [30]. The horizontal dimension of the field of view is 570 μm. (c) (bottom) contains the Fourier spectrum computed from the pattern in (a).

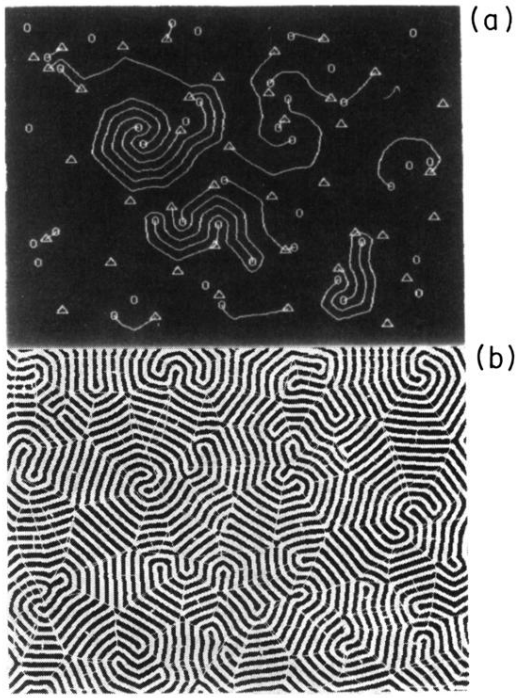

FIG. 8. Interlocking spirals, illustrated in the upper left quadrant of (a) (top), are frequently observed in branched labyrinths. They give rise to a "rosette" structure in the pattern morphology, exemplified by (b) (bottom): "Segment clusters" share the core of the spiral as a common vertex [23,30]; the left portion of another rosette structure is visible near the right-hand edge of the figure. These structural features are very prominent in color-coded images [23]. The horizontal dimension of the field of view is 570 μm.